Integrated UAS and LiDAR reveals the importance of land cover and flood magnitude on the formation of incipient chute holes and chute cutoff development

Quinn W. Lewis,[1,2]* (iD) Douglas A. Edmonds[1] and Brian J. Yanites[1] (iD)
[1] Department of Earth and Atmospheric Sciences, Indiana University, Bloomington, IN 47405, USA
[2] Department of Geography and Environmental Management, University of Waterloo, Waterloo, OntCanada

*Correspondence to: Quinn W. Lewis, Department of Geography and Environmental Management, University of Waterloo, Waterloo, Ont., Canada. E-mail: quinn.lewis@uwaterloo.ca

ESPL

Earth Surface Processes and Landforms

ABSTRACT: Meandering river sinuosity increases until the channel erodes into itself (neck cutoff) or forms a new channel over the floodplain (chute cutoff) and sinuosity is reduced. Unlike neck cutoff, which can be measured or modelled without considering overbank processes, chute cutoff must be at least partially controlled by channel-forming processes on the floodplain. Even though chute cutoff controls meandering river form, the processes that cause chute cutoff are not well understood. This study analyses the morphology of two incipient chute cutoffs along the East Fork White River, Indiana, USA, using high temporal and spatial resolution UAS-based LiDAR and aerial photography. LiDAR and aerial imagery obtained between 1998 and 2019 reveals that large scour holes formed in the centre of both chutes sometime after chute channel initiation. A larger analysis within the study watershed reveals that scour holes within incipient chutes can be stable or unstable, and tend to stabilize when the chute is colonized by native vegetation and forest. When the scour holes form in farmed floodplain, they enlarge rapidly after initial formation and contribute to complete chute cutoff. In addition, this study shows that the formation of scour holes can occur in response to common, relatively low-magnitude floods and that the amount of incipient chute erosion does not depend on peak flood magnitude. The role of scour holes in enlarging chute channels could be an important mechanism for chute channel evolution in meandering rivers. This study also confirms that understanding the relationships among flow, land cover, and cutoff morphology is substantially improved with on-demand remote sensing techniques like integrated UAS and LiDAR. © 2020 John Wiley & Sons, Ltd.

KEYWORDS: LiDAR; chute cutoff; meandering river; UAS; drone

Introduction

Meandering rivers constantly alter their form by eroding sediment along their outer banks at bends, and depositing sediment on their inner banks (Leopold and Langbein, 1966; Lawler, 1993). As meandering river channels evolve, the total channel length compared to valley length, a variable that defines river sinuosity, increases (Schumm, 1963; Stølum, 1996). Sinuosity does not increase infinitely, because at some point channel cutoff occurs and decreases the total length of the river channel. The process of channel cutoff regulates meandering river planform (Hooke, 1995; Camporeale *et al.*, 2008; Micheli and Larsen, 2011), and results in oxbow lakes when the former channel bend becomes fully disconnected from the river during non-flood flows (Howard and Knutson, 1984). Cutoffs can also mobilize massive amounts of sediment into the downstream channel and can thus result in both erosion of channel-adjacent land and rapid in-channel sedimentation (Zinger *et al.*, 2011; Schwenk and Foufoula-Georgiou, 2016). Loss of floodplain land can be particularly damaging for society, because

floodplains are productive and valuable for farming (Orr *et al.*, 2007; Opperman *et al.*, 2010). Oxbow lakes are also ecologically important, altering floodplain surface and groundwater connectivity that partially control floodplain habitat characteristics, nutrient sequestration, and floodwater retention (Constantine and Dunne, 2008). Despite the hydrologic, ecologic, and societal importance of cutoffs, there is a lack of information on mechanisms that lead to their initiation, growth, and ultimate capture of flow from the main channel (Viero *et al.*, 2018).

River cutoffs are typically classified into two types: (1) neck cutoff, where the channel migrates into itself without the formation of a new channel (Gagliano and Howard, 1984); and (2) chute cutoff, where a channel longer than the mean channel width forms within the floodplain across the bend (Hooke, 1995; Constantine *et al.*, 2010). Individual channel cutoffs might be some combination of these classes (Hooke, 2004), but in general neck and chute cutoffs are thought to be driven by different dominant processes (Howard and Knutson, 1984; Gay *et al.*, 1998; Richards and Konsoer, 2019). Because neck cutoffs are not associated with a newly formed channel across
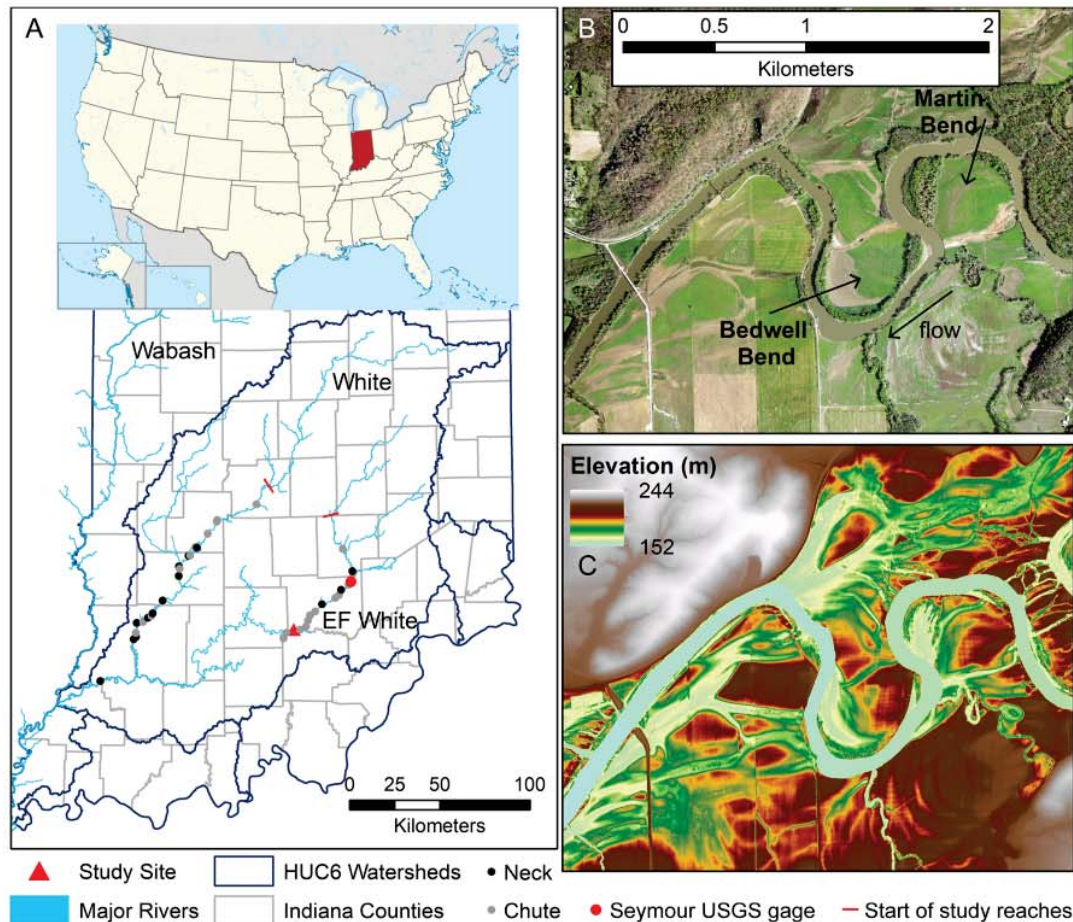
Figure 1. (A) Location of 37 cutoffs since the mid-1940s in Indiana, study sites Martin and Bedwell Bends near Sparksville, IN, and inset of Indiana's location within the United States. Frames (B) and (C) show a 2017 aerial photograph and a 2011 LiDAR of the surrounding floodplain, respectively. [Colour figure can be viewed at wileyonlinelibrary.com]

the bend, in-channel processes such as bank erosion and near-bank groundwater processes, such as sapping, are thought to control their occurrence (Camporeale *et al.*, 2008; Han and Endreny, 2014). Neck cutoffs can be parameterized and modelled without directly considering floodplain morphology and flow (Han and Endreny, 2014). In contrast, chute cutoffs must be caused by channel-forming processes on the floodplain and as such are less suitable for model parameterization because they depend partly on the erodibility and heterogeneity of the floodplain (Constantine *et al.*, 2010; Viero *et al.*, 2018).

Understanding chute cutoff formation in natural rivers has been challenging because it is difficult to predict when and where an incipient chute channel will form, and once initiated, the rapid change of the channel and floodplain does not easily allow for systematic, process-based field measurements (Zinger *et al.*, 2011; Viero *et al.*, 2018; Li *et al.*, 2019). Instead, the process is most often inferred from changes in river morphology over time. Studies of chute cutoff form and the processes that could lead to cutoff initiation and eventual flow capture have resulted in the development of three main classes of chute cutoff (Constantine *et al.*, 2010): (1) downstream extension of embayments or erosional inlets formed by strong, erosive flow on the outer bank of a sharp meander bend; (2) headward incision of a proto-channel through the bend; and (3) the capture of the main flow by existing swales present along extending point bars. Much of the evidence for these chute cutoff classes is inferred from imagery and the form of the incipient chute before cutoff occurs, rather than from direct measurements of flow and erosion during

the event that cuts off the bend. For example, it is unknown why some bends might form an erosional embayment that leads to a cutoff while others do not (Constantine *et al.*, 2010), and there is limited mechanistic understanding of how and where proto-channels form and grow upstream within the floodplain (Gay *et al.*, 1998). Thus, the driving physical processes that eventually cause channel enlargement and capture for each class are not known, and a lack of detailed descriptions of evolving chute cut-offs hinders a deeper understanding of chute cutoff dynamics (Van Dijk *et al.*, 2014; Eekhout and Hoitink, 2015).

Recent advancements in unmanned aerial systems (UAS) and light detection and ranging (LiDAR) technologies could fill this gap because they allow for both high spatial and high temporal resolution monitoring of morphologic change (Lejot *et al.*, 2007; Tarolli, 2014; Woodget *et al.*, 2017) and could be useful for improving our understanding of river cutoffs. Photogrammetry derived from UAS has been used to characterize erosion of rivers (Lejot *et al.*, 2007; Carbonneau and Dietrich, 2017), and analysis of channel change from LiDAR data is commonplace in studies of fluvial environments (Charlton *et al.*, 2003; Milan *et al.*, 2007; Mason and Mohrig, 2018). However, until recently it has not been feasible to integrate LiDAR with small UAS (Anderson and Gaston, 2013; Colomina and Molina, 2014). UAS and Li-DAR integration allows for high levels of flexibility, allowing researchers to set the spatial and temporal resolutions of acquired data within the technical abilities of the instruments. LiDAR affixed to UAS can be accurate to within a few centimetres and does not always require surveying ground control points, which
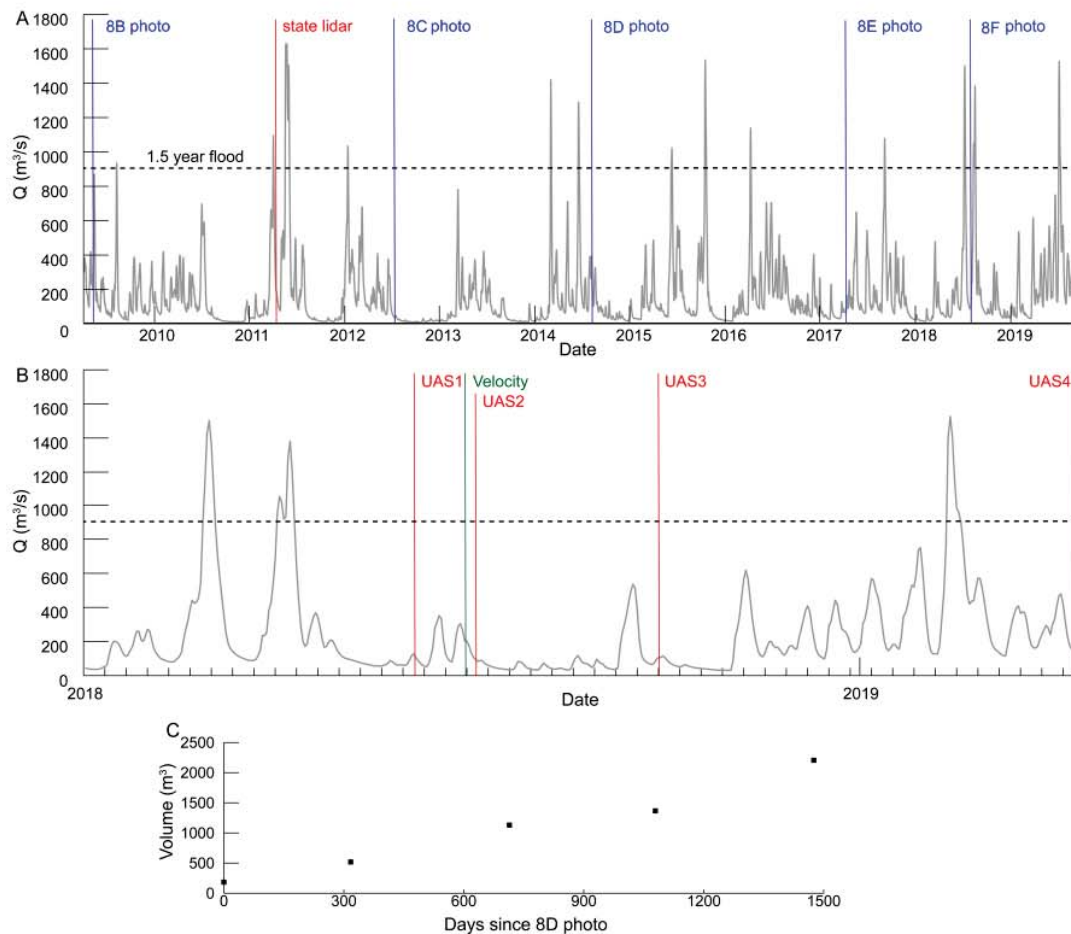
Figure 2. Flow at the USGS stream gauge at Seymour, IN over the last 10 years (A) and since 2018 (B). The red lines show when the LiDAR was obtained, and the blue lines show the dates of aerial photos shown in Figure 8. The estimated eroded volume of the large hole in Bedwell Chute since photo 8D is shown in (C). [Colour figure can be viewed at wileyonlinelibrary.com]

might be important for actively changing fluvial environments that could erode semi-permanent installations. A UAS integrated with LiDAR and a camera can produce both photogrammetry and LiDAR point clouds, allowing for independent verification of results. Integrating multiple sensors on a single UAS also allows use of one method over another during certain conditions, such as using LiDAR instead of photogrammetry when vegetation obscures the ground. UAS and LiDAR should thus increase the capabilities of researchers to characterize fluvial morphology in detail. These technologies could drastically improve our understanding of cutoff processes.

In this paper we analyse a previously undescribed chute erosion mechanism – the formation and evolution of channel-scale scour features within incipient chute channels on the floodplain. We use a LiDAR-equipped UAS to obtain high-resolution topography of two chute channels along the East Fork White River in Indiana, USA across a range of inundation events in the chute. We describe the methodological considerations and accuracy of the integrated LiDAR-equipped UAS. We also use an acoustic Doppler current profiler (ADCP) and large-scale particle image velocimetry (LSPIV) to measure velocity within one of the chute channels during a flood. These combined morphological and velocity measurements are used to infer the physical processes that drive the formation and evolution of the two chute channels. Aerial photography from both the LiDAR-equipped drone and from extant programmes is used to support the direct morphologic change analysis and more completely understand the impacts

of similar scours along the East Fork White and West Fork White Rivers in Indiana. The formation of scours on incipient chutes is not easily categorized by existing conceptual theories of chute cutoff formation, and we discuss their potential formative factors.

Study Site

Two incipient chute cutoffs in farmed fields along the East Fork White River near Sparksville, IN were used as case studies to measure incipient chute channel morphologic change in detail (Figure 1). Martin and Bedwell Bends are back-to-back meander bends, roughly similar in planform, which have evolved slowly from simple sine-like bends in the mid-1940s to their current compound bend planform (Figure 1). Bankfull channel widths of the bends are around 90 m, and bankfull channel depths range from 3 to 4 m. Both bends contain incipient chute channels cutting into floodplains characterized by clay- and organic-rich topsoil, which are farmed annually for soybeans or corn. The beginnings of both chute channels were first visible on aerial photographs taken in 1998.

The East and West Fork White Rivers drain into the Wabash River along the Southern Indiana–Illinois border, and together the three river systems drain much of the state of Indiana (Figure 1). Since the first aerial photographs of Indiana in the mid-1940s, 37 cutoffs (23 chute and 14 neck) have occurred in the downstream portions of the East Fork White and White
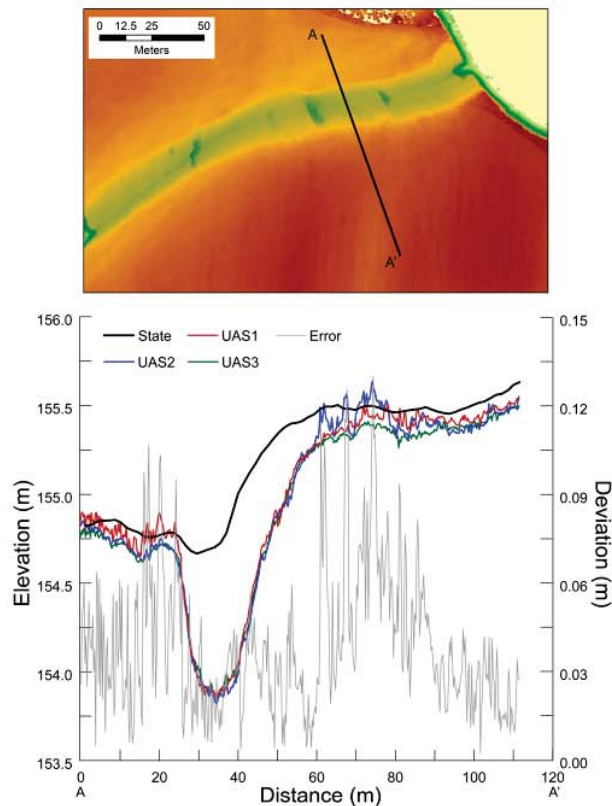
Figure 3. Comparison between state LiDAR and UAS-derived LiDAR across the upstream portion of Bedwell chute. The top panel shows the extraction location of the cross-section. The deviation is calculated as the standard deviation between the first three UAS flights. [Colour figure can be viewed at wileyonlinelibrary.com]

Rivers (Figure 1, downstream of red lines). The lack of control structures and the common occurrence of cutoff suggests both rivers are not managed by flow control structures. The average daily flow at the US Geological Survey (USGS) stream gauge at Seymour, IN (03365500) (the closest regularly monitored gauge to Bedwell and Martin Bends) between 1927 and 2018 is 77 $m^3 s^{-1}$, the 1.5-year flood is 897 $m^3 s^{-1}$, and peak flows most often occur in spring. Based on flow modelling, the East Fork White River floods frequently – there is water in the low-lying floodplain channels every 19 days on average (Czuba et al., 2019).

Methods

Incipient chute and floodplain morphology at Bedwell and Martin Bends was obtained from a combination of sources. State-wide LiDAR data was obtained for the study site in 2011 and is the earliest morphological condition of each chute. Using a LiDAR-equipped UAS, we acquired morphology on 5 and 7 June 2018 for Bedwell and Martin chute, respectively (UAS1). A second scan was performed at both bends on 4 July 2018, after a flood event which inundated the chutes (UAS2), and a third scan was performed at Bedwell chute on 19 July 2018, during a low flow but after heavy local precipitation (UAS3). A final scan (UAS4) was performed on 10 April 2019, to obtain roughly a full year of potential morphologic changes at the chutes (Figure 2).

We measured 11 velocity cross-sections within Bedwell chute using a TRDI RiverRay ADCP during a small flooding event (preceding UAS2) on 14 June 2018. We pulled the ADCP, mounted in a TRDI catamaran, across the chute channel six times at each cross-section. ADCP data post-processing was performed in the Velocity Mapping Toolbox (VMT – Parsons et al., 2013). Due to strong velocity gradients and flow complexity within a large hole, large-scale particle image velocimetry (LSPIV) using PIVLAB was used to supplement ADCP cross-sections (Thielicke and Stamhuis, 2014; Lewis and Rhoads, 2018). Although the LSPIV results cannot be used to analyse flow below the water surface, the high spatial resolution is used to better place the ADCP cross-sections into context and obtain details in high spatial resolution on flow within the hole. Velocity was obtained from a 30-s portion of a video, obtained at 30 Hz in 4 K resolution (3840 × 2160 pixels) from a DJI Phantom 4 UAS. Thirty seconds has been shown to be long enough to avoid biases from wind or lack of consistent patterns within the PIV interrogation area (Lewis et al., 2018).

UAS methodology – instrumentation and accuracy

Instrumentation

LiDAR and aerial photography were obtained from a DJI M600 hexacopter UAS, which was customized by Phoenix LiDAR Systems and outfitted with a Reigl MiniVux LiDAR unit and a Sony A6000 digital single-lens reflex (DSLR) camera (Figure 3). A Northrup-Grumman inertial measurement unit (IMU) and a CHC global positioning system (GPS) were integrated with the camera, UAS, and LiDAR. The LiDAR point accuracy in x, y, and z dimensions is about 0.2–0.3 cm at a distance of 75 m based on a borehole siting test performed on the system by the manufacturer. The LiDAR point cloud was acquired during flight using software provided by Phoenix LiDAR Systems.

The final accuracy of the point cloud and aerial photographs produced with the integrated system are dependent on the GPS base station accuracy. During each flight, the base station was set up in an arbitrary location and recorded data for at least 2 h to obtain a static solution when submitted to the Online Positioning User Service. The GPS data was not used to correct the location of the UAS in real time, but rather was used in conjunction with the on-board IMU to create an accurate UAS trajectory file in the post-processing stage. The accuracy of the GPS control point determined after OPUS correction was typically between 0.5 and 1.5 cm in the x and y direction, and 1–2 cm in the z direction. Occupying the arbitrary GPS point for longer, or occupying a benchmark, could have improved the accuracy but limited the flexibility of the system and was deemed unnecessary for this study. Factors like wind and vegetation presence also impact the overall accuracy of LiDAR and aerial photograph data. Additional processing of the LiDAR point cloud, including determining ground-designated returns, was performed in the TerraSolid software suite. Post-processing ground surface adjustment resulted in small improvements in the LiDAR point cloud relative accuracy (i.e. decreases in root mean square error among surfaces obtained from the same flight), yet could not improve absolute accuracy (i.e. the location of points in real-world coordinates).

Accuracy

To assess the accuracy of the UAS-LiDAR-derived digital elevation models (DEMs), we compared the elevations of a line across a stable section of Bedwell chute among the state LiDAR and UAS scans 1–3 (Figure 3). No manual editing of the point cloud or DEMs was performed to better assess the true data quality provided by the instrument. We produced 0.25 m spatial resolution bare-earth DEMs within the chute channels at both sites, which contained around 100 points m^{-2}. Repeat measurement of the same ground-surface transect DEM within
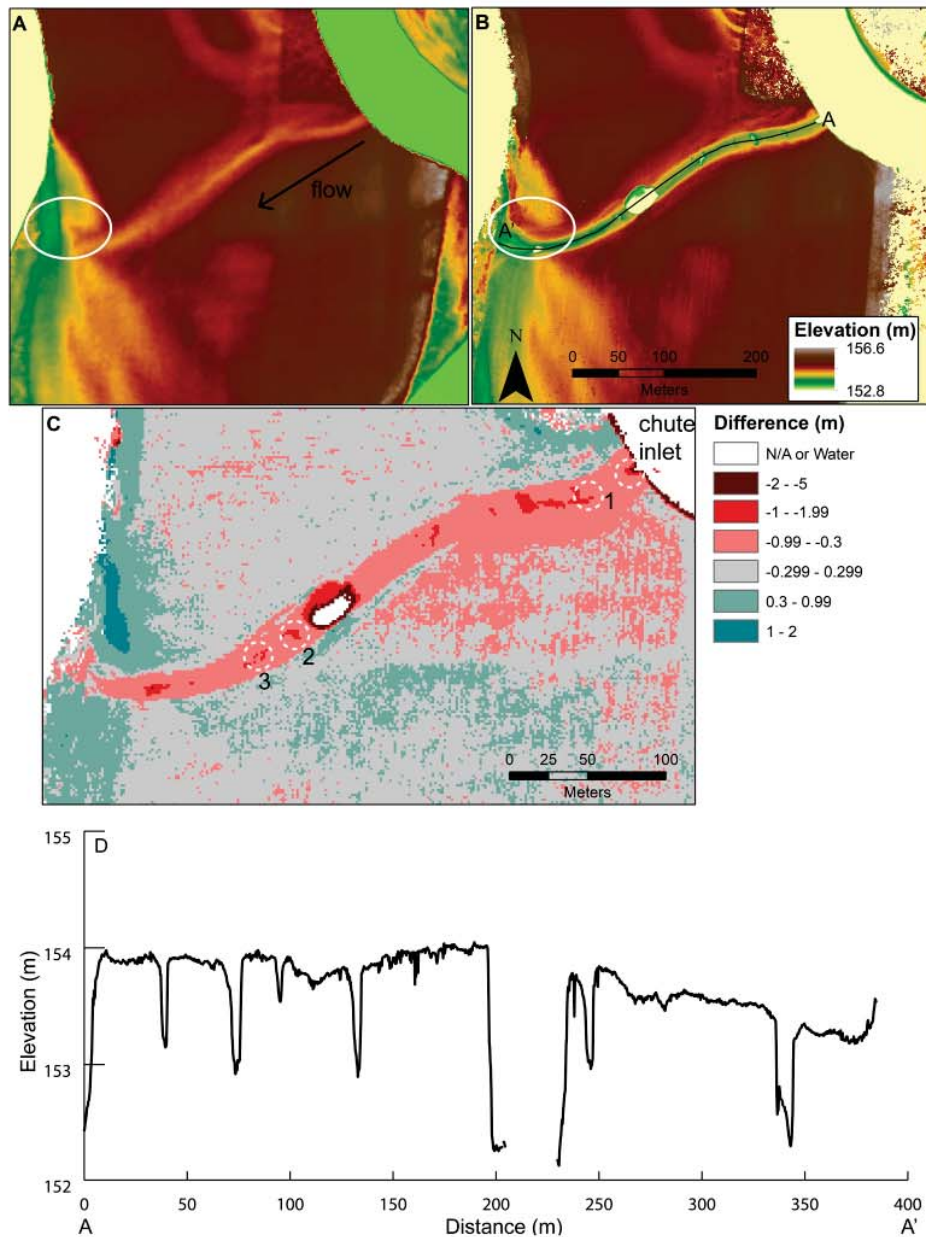
Figure 4. Change in topography of Bedwell chute from 2011 (LiDAR, A) to 5 June 2018 (UAS1, B). Formation of scour holes within the cutoff is shown in the DEM-of-difference (C). The labelled white circles in (C) are shown in more detail in Figure 7. A profile from A to A' in (B) shows the presence of major and minor scour holes (D). Note that no DEM smoothing was performed. The white ellipse highlights the region of deposition along the right bank of the chute channel. [Colour figure can be viewed at wileyonlinelibrary.com]

Bedwell chute revealed precision to within <5 cm (Figure 4; black line is the location of the transect). On the chute margins, low-lying vegetation present during UAS1 and UAS2 campaigns created noisy DEMs that placed bare earth higher than the UAS3 measurement, when the field adjacent to the chute had just been ploughed and seeded so that no vegetation was present. Standard deviations among the three UAS measurements peaked around 12 cm within the low-lying vegetation (Figure 3). Because of the lack of vegetation, the differences among the UAS-derived DEMs within the chute are substantially smaller. Elevation deviations are generally around 3 cm, which is near what would be expected given instrument limitations (Figure 3). Given the potential presence of low-lying vegetation, and the variable states of the farm field surrounding the chutes (i.e. ploughing and planting), we assumed a

conservative value of 30 cm to identify real landscape change among the UAS-LiDAR measurement campaigns.

Results

Morphologic change and aerial photographs

Bedwell Bend
In 2011, when the state-wide LiDAR was acquired, the incipient Bedwell chute was well developed but there was no evidence of a large scour hole (Figure 4A). Topography collected 7 years later from UAS1 revealed that a series of seven scour holes formed throughout the chute channel (Figures 4B–D). In the centre of the chute channel there was a large scour hole
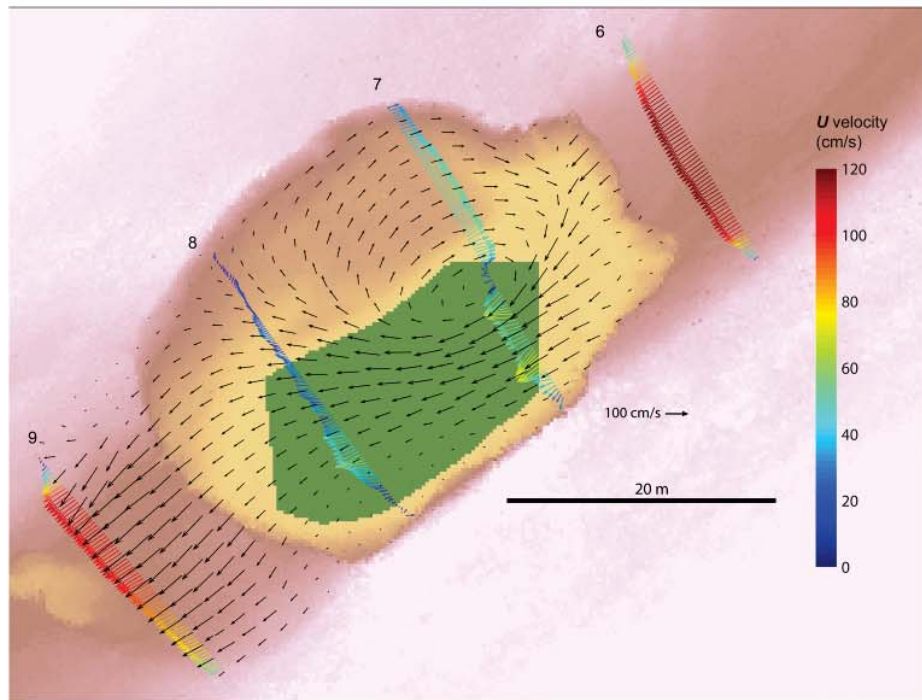
Figure 5. LSPIV velocity vectors overlying ADCP depth-averaged velocity in the large hole at Bedwell chute. [Colour figure can be viewed at wileyonlinelibrary.com]
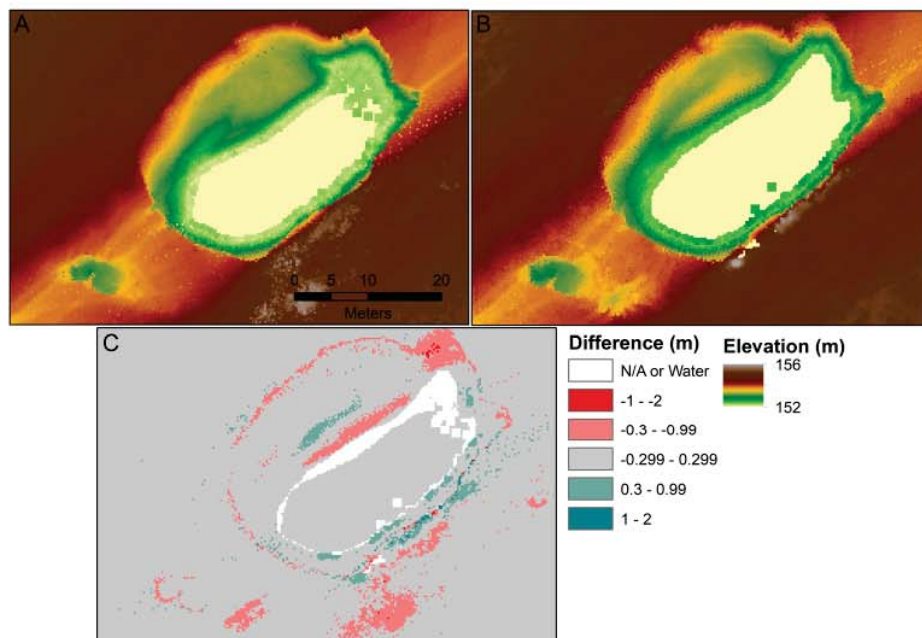

Figure 6. Change in morphology of large hole within Bedwell chute from UAS1 (A) to UAS2 (B), captured with UAS LiDAR. Change within the large hole is shown in the DEM-of-difference (C). Note that no DEM smoothing was performed. [Colour figure can be viewed at wileyonlinelibrary.com]

about 3 m deep with a water level roughly the same elevation as the main channel, and upstream and downstream of that there were smaller holes between 0.3 and 0.6 m deep that did not contain water (Figure 4B). A small embayment formed at the upstream entry of the incipient chute and extended about 10 m downstream along the chute from the main channel outer bank (Figures 3A and 4). The farmed parts of the floodplain surrounding the incipient chute did not change enough to quantify. Substantial sediment deposition occurred on the right side of the downstream portion of the chute channel as the

chute re-entered the main channel (white circle in Figures 4A and B).

On 14 June 2018, a small flood on the East Fork White River peaked at the Seymour gauge at roughly 340 m^3 s^{-1} (Figure 2). ADCP data were obtained at 11 cross-sections through the chute on 15 June 2018 when flow had fallen to 227 m^3 s^{-1}. Flow depths within the chute ranged from about 1 to 4 m within the large scour hole. Total discharge through the chute was roughly 12 m^3 s^{-1}. Flows both upstream and downstream of the large hole reached depth-averaged velocity maxima of
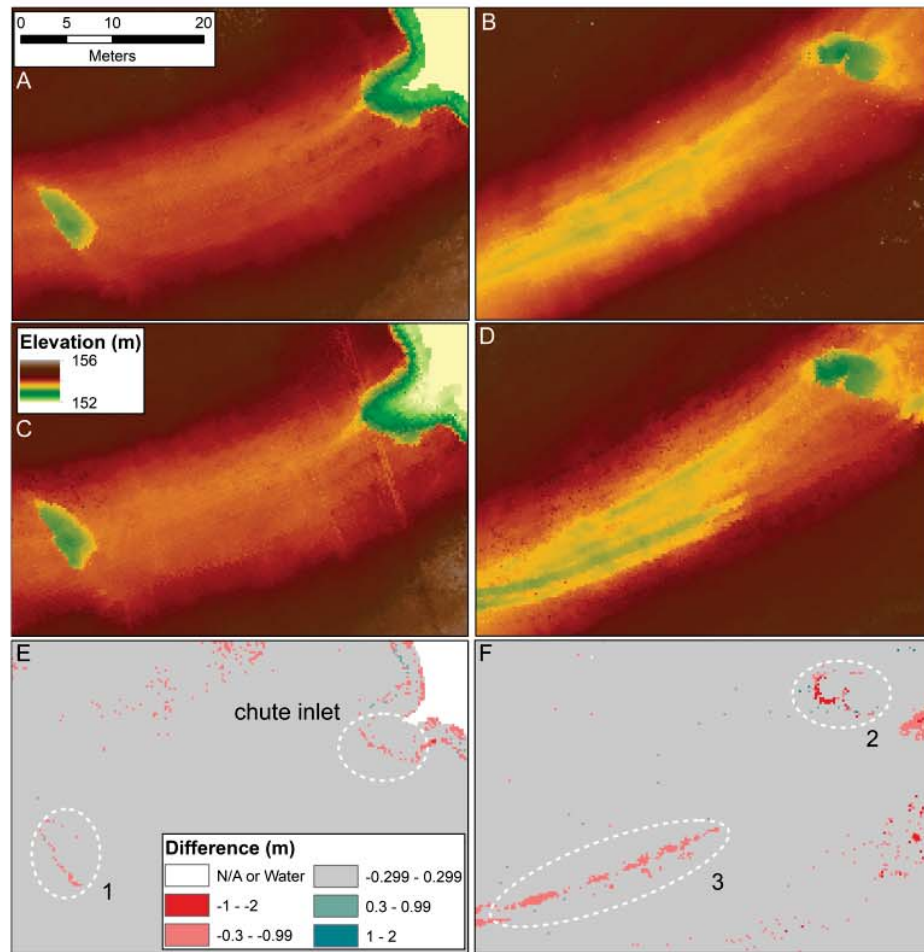
Figure 7. Change in morphology of the upstream small hole and the cutoff inlet from 4 June 2018 (A) to 5 July 2018 (C), and change in morphology of a downstream hole from 4 June 2018 (B) to 5 July 2018 (D) captured with UAS LiDAR. Change is shown in the DEM-of-difference (E, F). The white ellipses show sections of erosion, and their locations are shown in Figure 4. Note that no DEM smoothing was performed. [Colour figure can be viewed at wileyonlinelibrary.com]

$1.2\,\mathrm{m\,s^{-1}}$, while flow in the large hole expanded and recirculated (Figure 5). LSPIV velocity vectors reveal that flow was forced to occupy only about one-third of the channel at cross-section 7 due to the large recirculation cell, but depth-averaged velocity remained low because of the vertical expansion of the flow area as it moved into the hole (Figure 5). As flow exited the large hole, it rapidly recovered to roughly the same velocity as upstream of the hole (Figure 5).

A second flood peak of roughly $283\,\mathrm{m^3\,s^{-1}}$ occurred on 23 June, and flow remained too high to capture channel morphology with the UAS LiDAR until the water from the second small flood receded. UAS2 was used to assess the change in chute morphology after the 15 and 23 June floods (Figure 2) that inundated the chute, and so any morphologic changes to the channel and holes are due to flow within the chute channel. Erosion occurred along the margins of the hole on all sides except for the left bank, where the highest velocities were focused (Figure 5). Expansion of the bar occurred within the section of the hole that was dominated by flow recirculation (Figure 6).

Although flow was moving at over $1\,\mathrm{m\,s^{-1}}$ during the ADCP measurement period and shear stresses ranged from 0.5 to $1.5\,\mathrm{N\,m^{-2}}$ over the measurement cross-sections, the other smaller holes changed very little between UAS1 and 2 (Figure 7). Only a very narrow section (around 1 m or less) of the downstream edge of the small holes eroded due to the two floods between UAS1 and 2. This sub-meter-scale erosion also

extended the embayment slightly from the main channel into the chute (Figure 7).

Most of the changes in the chute as measured from the UAS LiDAR occurred in and around the scour holes, which indicates that erosion was likely caused by discrete detachment of the cohesive bed material (Istanbulluoglu *et al.*, 2005). Shear stresses of $1\,\mathrm{N\,m^{-2}}$ should be able to mobilize coarse sand of about 1.2 mm diameter (Wiberg and Smith, 1987; Moody *et al.*, 2005), which is larger than the surface sediment in this area, yet there were no noticeable changes of the chute bed between UAS1 and 2. Because the chute bed is located in cohesive, farmed floodplain sediment, the bed approximates the conditions of a bedrock channel (Moore and Masch, 1962; Istanbulluoglu *et al.*, 2005), and thus the bed is likely to be eroded during large detachment events. Shear stresses are concentrated on the downstream lips of the holes, where strong turbulence and flow that must move vertically over the lip is more likely to pull cohesive sections of the bed material away from the hole wall.

We can also constrain the formation and expansion rates of the scour holes before our measurements with historical aerial imagery. The first clear evidence of the incipient chute channel at Bedwell Bend is in an aerial photograph taken on 26 March 1998, and by 2005 the chute channel clearly conveys floodwater (Figure 8). National Agriculture Imagery Program (NAIP) aerial photography acquired on 7 June 2012 at Bedwell Bend

Figure 8. Aerial photographs of Bedwell Bend from: March 2005 (A), April 2009 (B), June 2012 (C), July 2014 (D), April 2017 (E), and 4 July 2018 (F, obtained with UAS). Flow is from right to left. See Figure 2 for image acquisition dates. [Colour figure can be viewed at wileyonlinelibrary.com]
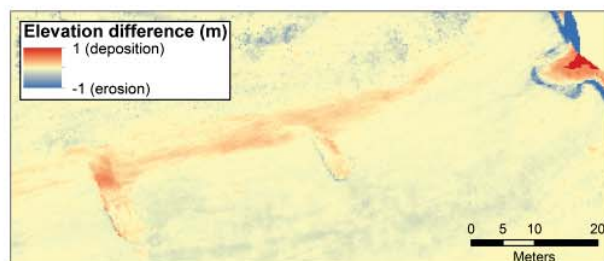

Figure 9. A DEM-of-difference between UAS1 and UAS4 focused on the upstream part of the chute. [Colour figure can be viewed at wileyonlinelibrary.com]

does not show evidence of any holes within the chute channel (Figure 8C). The next photograph, taken on 5 July 2014, shows that the large scour hole has formed and is about 6 m wide by 13 m long (Figure 8D). On 9 March 2017, smaller holes initiated along the chute (Figure 8E) and the large hole had grown to 20 m by 29 m in width and length, respectively. Presently, as determined from UAS2, the size of the hole is approximately 26 m wide by 36 m long. Measurements from all available aerial photographs reveal a roughly linear trend of growth in area of the large scour hole with time since initial formation (Figure 2).

The initial formation of the central scour hole must have occurred sometime between aerial photographs taken on 7 June 2012 and 5 July 2014. We know that a flow of around

$300 \, \mathrm{m \, s^{-3}}$ at the Seymour USGS gauge inundates the Bedwell chute (as determined from aerial photographs, the velocity measurements taken on 15 June 2018, and pressure transducers at the site). Considering this, there have been 34 floods that inundate Bedwell between the 2011 state LiDAR and UAS4. Between 7 June 2012 and 5 July 2014 (between which times the large hole formed), 11 inundation floods occurred. The highest peak flood that may have formed the hole within this period, occurring on 24 December 2013, was $1486 \, \mathrm{m^3 \, s^{-1}}$ and is the 16th highest flow on record since 1927. A flood of this magnitude has historically occurred on average about every 5 years, and has occurred 14 times since the first aerial photography in the mid-1940s.

From UAS1 and 4 there were eight overbank floods, yet there was little discernible change to most of the chute, with the exception of near the scour holes (Figure 9). The downstream margins of the scour holes eroded slightly, and the margins of the upstream incipient chute showed small amounts of deposition – perhaps due to sediment diffusion into the chute (Figure 9). The peak flow between these UAS-LiDAR scans was roughly $1500 \, \mathrm{m \, s^{-3}}$, essentially the same as the largest flow between the pre- and post-large-hole development images. In addition, while even small floods can change the morphology of the holes slightly within the chute, a full year of overbank flows did not alter the chute morphology substantially – even though the peak flood during our measurement period was similar in magnitude to peak floods that resulted in erosion of >1 m since 2011 (Figures 2 and 4). Overall, the flood or floods that initiated
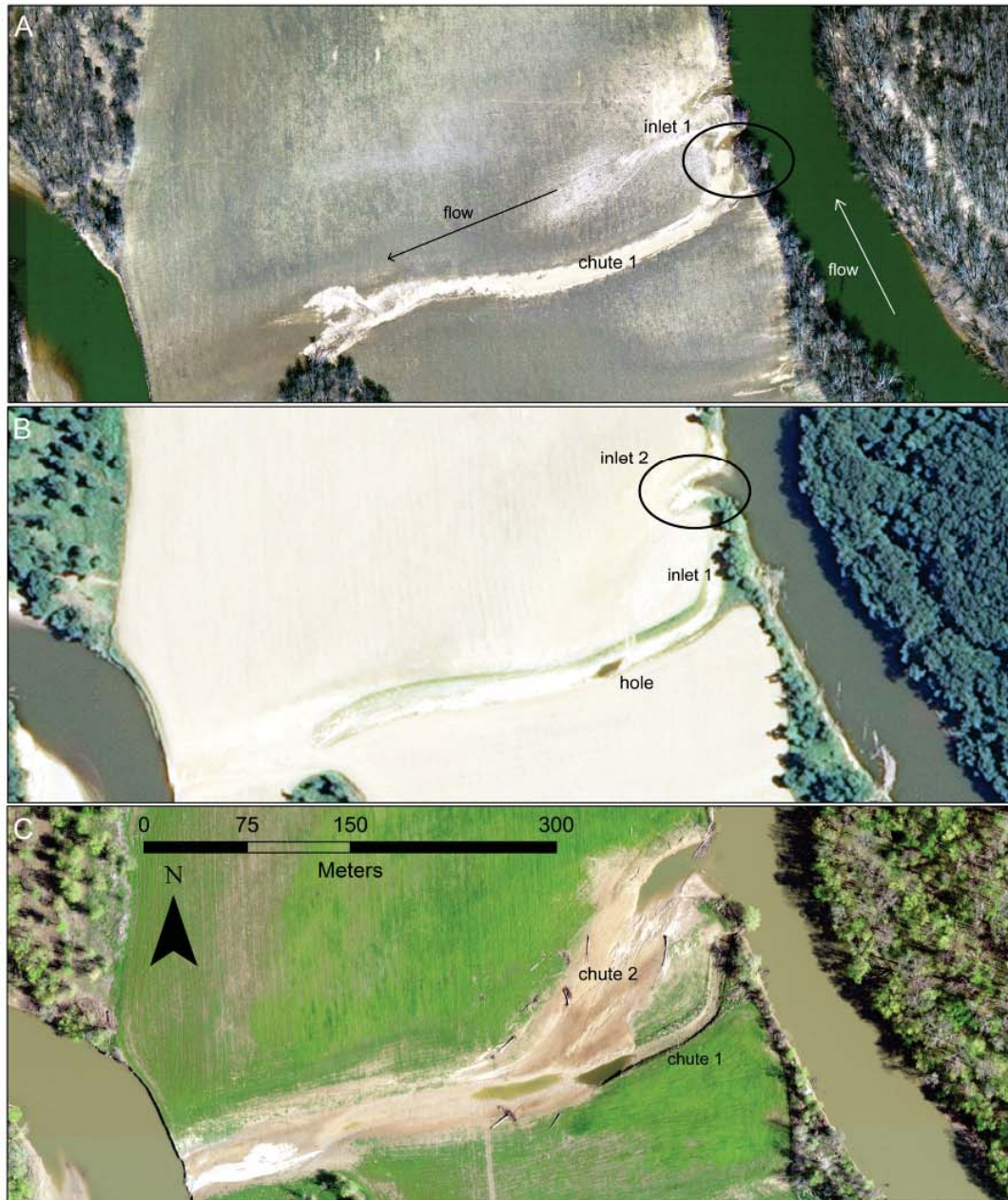
Figure 10. Aerial photographs of Martin Bend cutoff from March 2005 (A), June 2012 (B), and April 2017 (C). [Colour figure can be viewed at wileyonlinelibrary.com]

the large scour hole were not exceptional (i.e. less than 10-year floods), which indicates that features like the large hole within Bedwell chute might not be related to exceptional flooding events.

Martin Bend

At Martin Bend, a narrow erosional inlet and chute channel was visible in an aerial photograph taken on 26 March 1998 (Figure 10A, labelled inlet 1 and chute 1). In response, the land-owner planted trees within and along the incipient channel. A centrally located large hole could first be seen in aerial photographs from 2012 and has grown slowly since (Figure 10B). A second erosional inlet located about 50 m downstream of the initial incipient channel has grown since 2005 and is now dominant (Figure 10C, labelled inlet 2 and chute 2). The sec-ond inlet currently appears to be the more active channel due to growth of the inlet and evidence of scour (Figure 11). The

two upstream channels of Martin chute join at the location of the large hole, before draining back into the main channel. At Martin Bend at the time of the 2011 state LiDAR acquisition, both chutes 1 and 2 were present (Figure 11). The downstream chute 2 was characterized by the presence of a large embayment attached to the main channel, which fits within the conceptual model of chute cutoff evolution (Constantine et al., 2010).

LiDAR obtained from UAS1 shows that chute 2 at Martin Bend has become dominant, with the channel widening to about 50 m and deepening by about 2 m (Figure 11). Chute 1 narrowed slightly and became deeper by about 0.75 m, and the floodplain surrounding the upstream chute appears to be characterized by net deposition. The planting and growth of trees by the farmer might have prevented sediment transport into the first chute, promoting deposition along the channel margins, thereby leading to net narrowing and deepening of
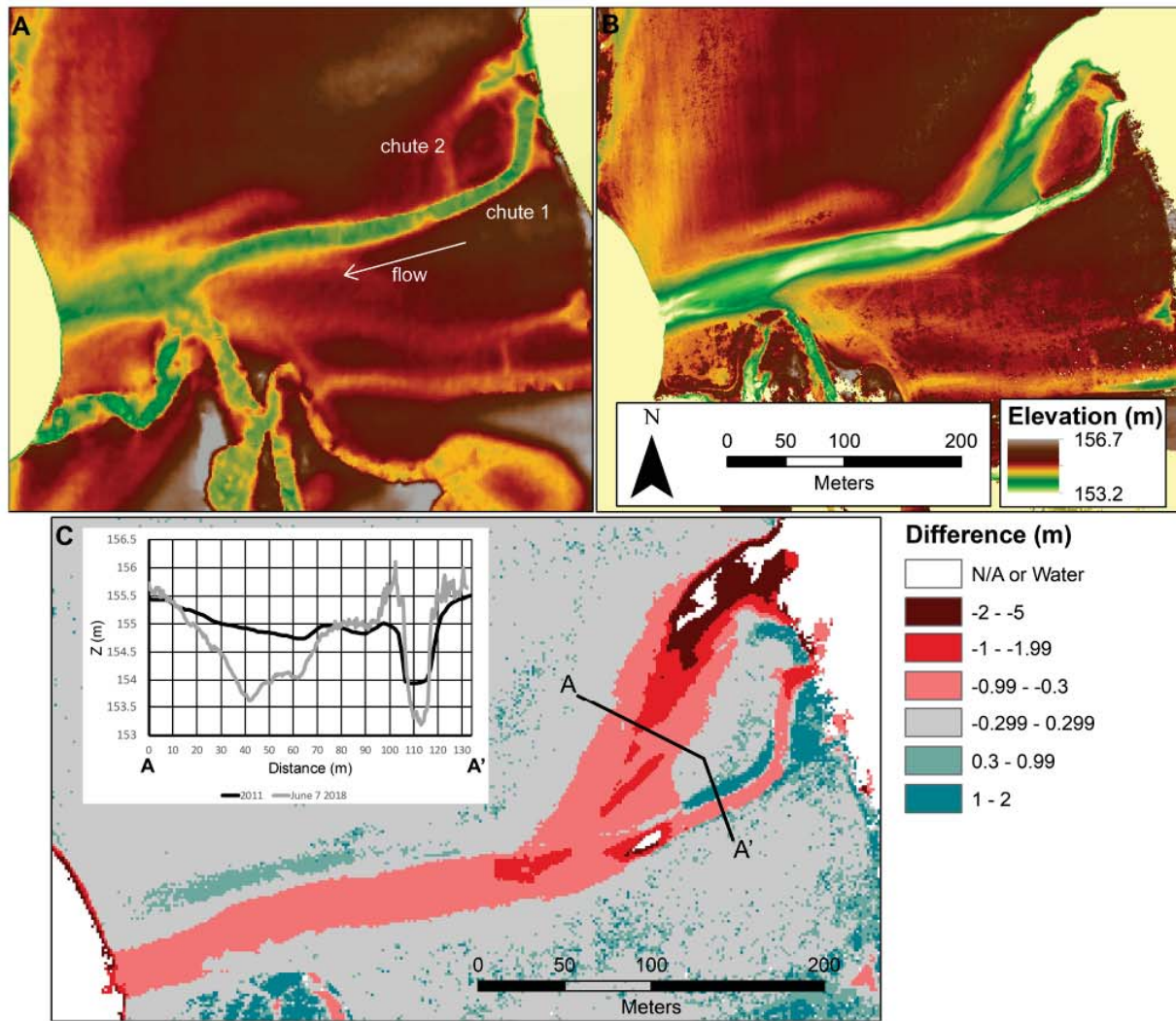
Figure 11. Change in topography of Martin cutoff from 2011 (state LiDAR, A) to 7 June 2018 (UAS1 LiDAR, B). Inset in (C) shows change within cross-section A to A′ plotted on the DEM-of-difference. Note that no DEM smoothing was performed. [Colour figure can be viewed at wileyonlinelibrary.com]

chute 1 (Allred and Schmidt, 1999). Chute 2 widened and deepened considerably between 2011 and 2018, and the large water-filled hole was present in the UAS1 scan. Although the

presence of a large hole in Martin chute is similar to Bedwell chute, there is no evidence of the presence of smaller holes within Martin chute. Subsequent UAS scans at Martin Bend
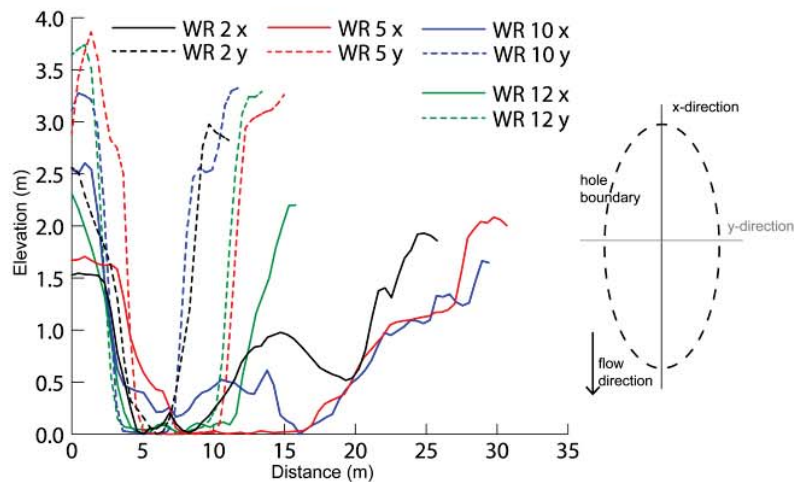

Figure 12. Scour hole streamwise (*x*) and transverse (*y*) morphology of selected holes (labelled 1–12 from upstream to downstream) along the West Fork White River. The definition sketch shows a simplified planview of hole morphology. [Colour figure can be viewed at wileyonlinelibrary.com]
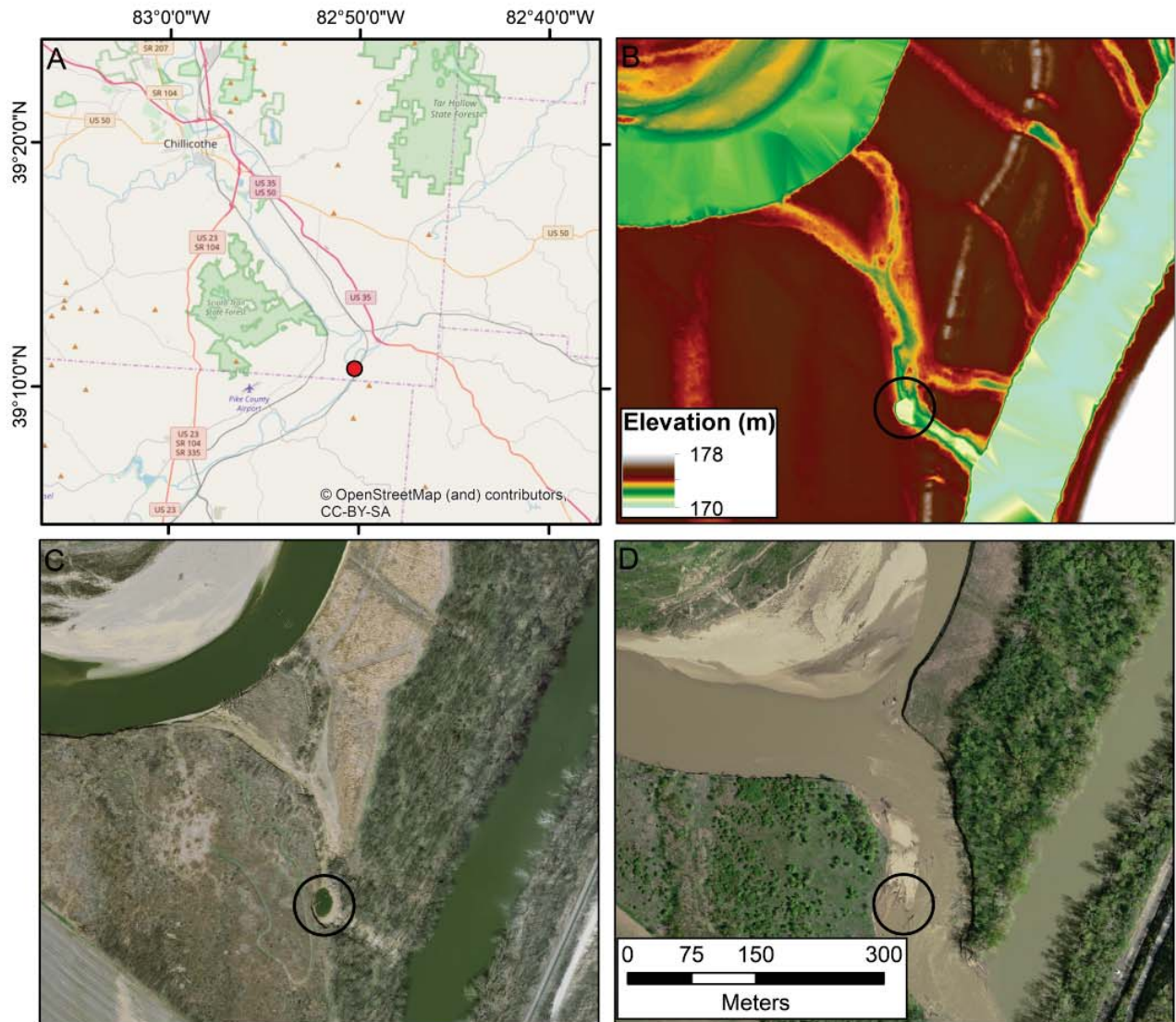
Figure 13. The presence of a scour feature (black ellipse) before a chute cutoff on the Scioto River in Ohio, USA (39°10′48.81″N, 82°50′15.35″W; map of location shown in frame (A)). LiDAR acquired in 2010 (B), aerial photo taken in 2011 (C), and aerial photo taken in 2013 (D). [Colour figure can be viewed at wileyonlinelibrary.com]
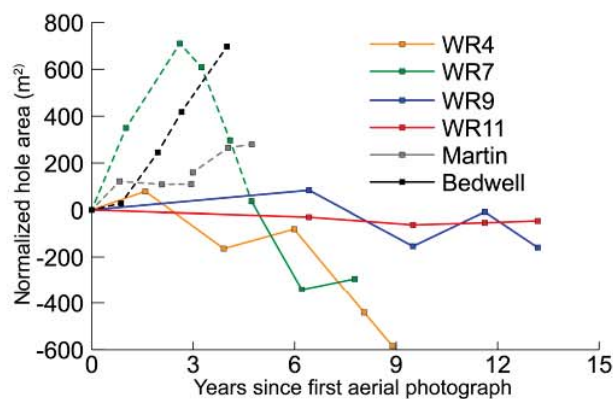

Figure 14. Change in scour hole area (measured from aerial photos) for selected holes within incipient chutes that have yet to cut off. Dashed sections of the lines are times for which the region around the hole is not forested (e.g. is cropped or grassland). Hole areas are normalized to the area when the first photograph was taken, such that the first measured area of the hole is set to 0 on the y-axis. [Colour figure can be viewed at wileyonlinelibrary.com]

revealed no noticeable changes in channel morphology, though standing water within the chute prevented full characterization by LiDAR. In sum, although Martin chute has a large hole, it also has an erosional inlet that is eroding downstream (Constantine *et al.*, 2010).

Similar features within the study watershed

Aerial photography accessed on Google Earth, combined with the 2011 state LiDAR DEM, was used to locate additional chute scour holes on the East and West Fork White Rivers. Including the Martin chutes, we identified 12 scour holes associated with chute channels in the 2011–2013 state LiDAR (Bedwell chute did not yet have a scour feature during LiDAR acquisition). These features were visually identified and cross-checked with aerial photographs, and only those features with discernible and obvious hole boundaries were considered. Many scour-like features contained water in aerial photographs, but LiDAR data showed low-sloped banks typical of swales or floodplain channels (David *et al.*, 2017), so they were not included. In
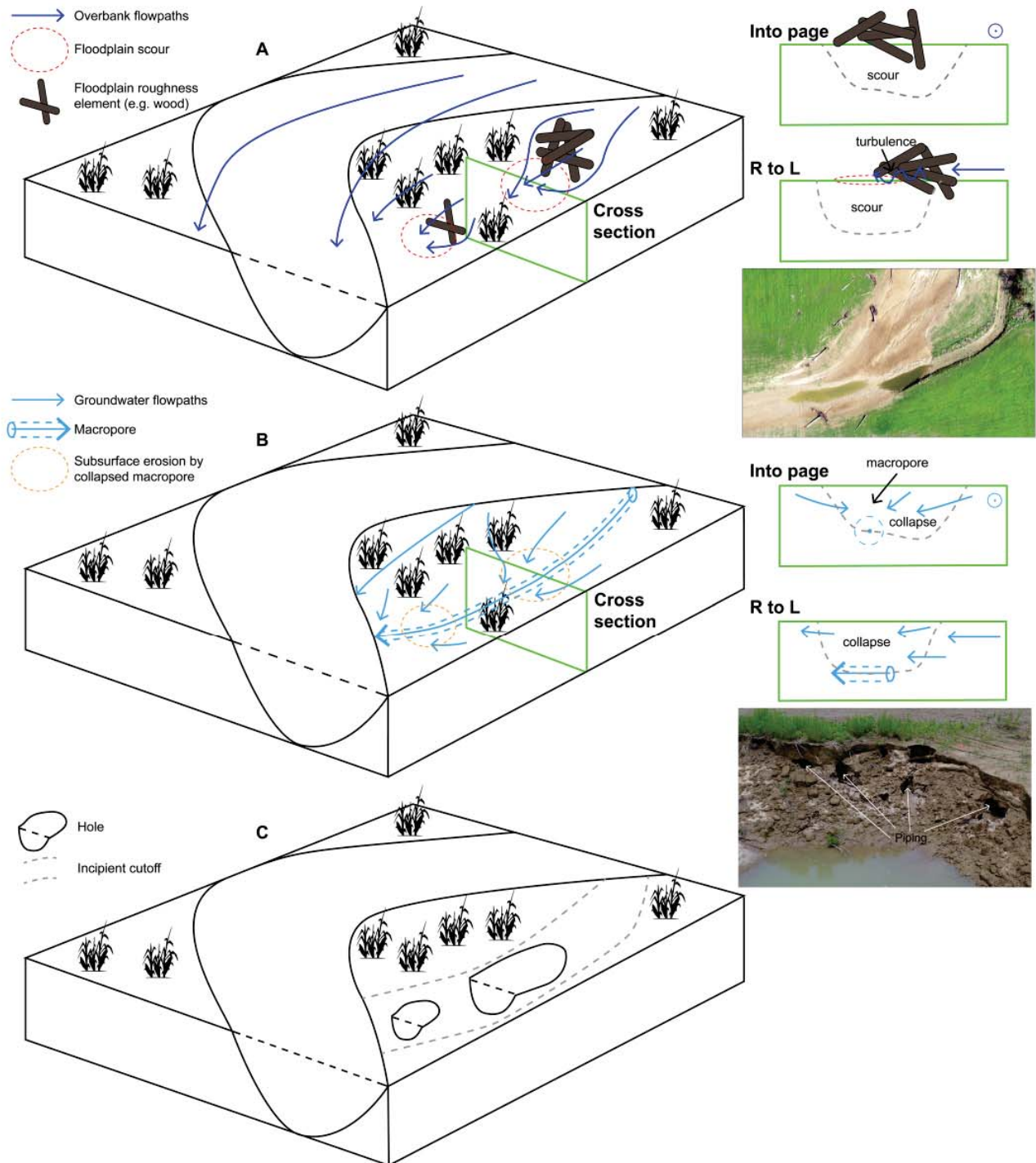
Figure 15. Two potential mechanisms for hole formation include (A) scour from overland flow and (B) erosion within and collapse of subsurface macropores and soil pipes. Either mechanism could produce the incipient chute morphology documented in this study and shown in (C). The inset photos show examples of each potential mechanism from Bedwell and Martin Bends. [Colour figure can be viewed at wileyonlinelibrary.com]

addition, the scour zones of some features were connected by a channel with a depth similar to the scour feature and were also not included. Finally, some additional chute scours could have existed prior to or after LiDAR acquisition, or could be too small to detect.

The scour holes have a longer streamwise-aligned (*x*) axis, with relatively steep slopes in the direction transverse (*y*) to the mean incipient chute streamwise flow direction (Figure 12). In the streamwise direction, the slopes are more gradual. A typical hole has higher transverse edges than streamwise edges, because the incipient channel has already been scoured slightly into the floodplain in the longitudinal direction (Figure 12).

Although we focused on two watersheds in Indiana, we expect these scour features to be present in rivers with morphology similar to the White and East Fork White. A similar large scour on the Scioto River in Ohio, USA – a river with bankfull widths around 100 m, bankfull depths about 4 m, and in a climate similar to the East Fork White River – was found within an incipient chute channel (Figure 13). Between two aerial photographs obtained in 2011 and 2013, the incipient chute fully cut off in the location previously occupied by the scour hole.

Discussion

The presence of large scour holes within evolving chutes appears to indicate instability within the chute and its surrounding floodplain. These scour holes enlarge through erosion along their margins and appear to form and grow in response to relatively common floods, as opposed to large-magnitude floods. Their presence and evolution have not been documented, yet they could play an important role in cutoff dynamics by either hastening cutoff or acting as markers of chutes that are nearing the completion of the chute cutoff process.

The potential importance of incipient chute scour features could be determined by the rate at which the feature grows. Constraining rates from aerial photographs show that two scour features were stable through time after initial formation, and two were associated with substantial reduction in area with time (Figure 14). Six scour holes (including Martin and Bedwell) were unstable and continued to increase in area, and three were in chutes that eventually cut off.

We find an interesting relationship between land cover/land use and the dynamics of these scour holes. Scour holes that grow are found in actively farmed fields, whereas stable scour holes that do not grow were found in forested areas (Figure 14). The presence of trees and vegetation provides additional shear resistance to the soil due to the presence of roots (Abernethy and Rutherfurd, 2001; Docker and Hubble, 2008). Vegetation is also an obstruction that slows floodplain flow (Aberle and Järvelä, 2013).

The morphological complexity of the chutes at Bedwell and Martin Bends illustrates the importance of using high spatial and temporal resolution datasets to better understand cutoff processes. It appears that many large scour features lead to rapid chute cutoff after their formation, meaning they are not persistent features visible in infrequently acquired photographs. The proliferation of 'on-demand remote sensing' methods, such as the UAS-based LiDAR system used in this study, will allow for improved understanding of the effects of relatively small and short-lived features on chute cutoff formation and evolution. The lack of previous research on scour holes within incipient chute channels might be partly related to the lack of spatial and temporal resolution of morphological datasets.

The style of chute cutoff formation observed in this study does not fit within previously documented models of chute formation (Constantine et al., 2010). The scour holes we observe are possibly important parts of chute channel growth and development. We see examples of chute channels that contain growing scour holes that can be unstable and ostensibly participate in cutoff completion in non-vegetated floodplains. The lack of a large embayment at Bedwell Bend, together with the formation of smaller scours within the chute, further suggests that the erosional process associated with unstable scour formation might need to be considered a fourth major mechanism of chute channel development (Constantine et al., 2010).

Our results show no strong correlation between flow and chute erosion processes, suggesting that existing conceptual models of cutoff formation might be further complicated (Gay et al., 1998). In this study the highest flow that occurred since the 2011 state LiDAR at Bedwell Bend was almost the same as the highest flow that was recorded between LiDAR scans from UAS1 and 4 (Figure 2). There was only slight erosion (focused on the margin of the holes) between UAS1 and 4 (Figure 12), yet since 2011 the chutes and Bedwell and Martin Bends eroded considerably and the large hole formed at Bedwell Bend. Thus, there is not a simple relationship between hydrodynamics and morphodynamics at our study sites, and the same flood can result in various morphologic responses. Although shear stresses within Bedwell chute during a small flood

were measured to be consistently over $1 \, \text{N} \, \text{m}^{-2}$, which is a reasonable stress to erode cohesive floodplain material, large floods may not result in considerably higher bed shear stresses and erosion. During major floods the entire floodplain near the chute is inundated, and the hydraulic gradient might be lower than during small floods that convey water through the chute but do not produce water on the floodplain (Eekhout and Hoitink, 2015). Additional research on the relationships among flood frequency, flood magnitude, and channel and floodplain morphology is needed to better understand and predict cutoffs in the field and to allow for appropriate modelling of chute cutoffs.

Conceptual model of scour hole formation in chute channels

The important question that remains is what forms these scour holes in chute channels. If we can better understand their formative processes, we can create predictive models that explain when they form and when they lead to chute channel cutoff. We suggest two distinct processes could lead to scour hole formation along the incipient chute channel. First, the chute could be formed mainly by scour from overland flow, where the holes represent regions of overland flow convergence, increased bed shear stress, and increased turbulence potentially caused by macro-roughness elements (Figure 15). For example, on Bedwell and Martin Bends, aerial photographs clearly show that large wood is deposited within the channel and floodplain, which results in surface gouging and scouring of floodplain sediment (Figure 15). Deposited trees and larger wood jams could act as obstacles to flow which cause increased flow velocity, relatively high vertical flow components (like flow over a step or a knickpoint), and elevated turbulence (Bressan et al., 2014). In addition, the hole at Martin Bend formed at the confluence of two distinct chutes (Figure 11). These factors could lead to high local shear stresses, which are required to detach and transport the cohesive soil- and clay-rich floodplain material (Moody et al., 2005). The formation of an initial small scour hole could further enhance vertical flow, turbulence, and thus shear stress during subsequent flow events and allow for the growth of the hole features and more clay detachment, as demonstrated at Bedwell Bend (Figures 7 and 9). Crucially, if this mechanism were dominating scour hole formation, we would expect larger flow events in the chute to cause more scour hole erosion. While our data do not clearly support this, we also note that woody debris, which would act as the local obstruction, does not appear to have long residence time within the chute.

The second potential formative mechanism is one dominated by subsurface flow. Substantial flow gradients between upstream and downstream of the chute, as well as subsurface flow convergence into pre-existing random low points within the floodplain and the incipient chute, should increase erosion and sediment transport via macropores and soil piping (Jones, 1971; Bernatek-Jakiel and Poesen, 2018). As the subsurface flow gradients reach a critical value, erosion might increase enough to cause a macropore to collapse and form the holes documented within the two chutes (García-Ruiz et al., 1997). The collapse then results in a local depression, which might increase in size due to additional pore failures, bank failures, and clay detachment. Evidence of soil piping into the large hole at the Bedwell chute supports the subsurface formative mechanism (Figure 15).

It is likely that both formative mechanisms act in concert, and the potential extension and growth of these holes are due

to both overland flow and subsurface processes. The holes present in Bedwell chute formed during a period without an exceptional flood, yet the same unexceptional floods were able to scour the channel into the floodplain between 2011 and 2018 (Figure 4). Peak flows might be deep enough to transport wood cleanly through the chute and remove existing wood, preventing the wood from anchoring in place and increasing local turbulence. In addition, a relationship between flood discharge and chute erosion could be complicated by the morphology of the chute itself. For example, a hole that reaches a critical size might trap a large portion of transported wood or focus most of the subsurface groundwater, and thus could become the locus of future erosion at the expense of the rest of the chute. The relationships among flood discharge, hydraulic gradients, cutoff morphology, and sediment transport should be the focus of future field research on cutoffs.

Conclusion

We studied the morphology of two incipient chute cutoff channels on the East Fork White River in Indiana, USA using aerial photography and LiDAR. Both Bedwell and Martin chutes were characterized by the formation of large scour holes. Hydrologic analysis of Bedwell chute revealed that the hole formed and grew substantially during a period without floods larger in magnitude than the 6.5-year flood. Additional smaller holes formed in Bedwell chute between LiDAR scans in 2011 and 2018, and the formation of all holes coincided with about 0.5 m of chute erosion and lowering. We also found similar features throughout the study watersheds, and suggest that the lack of documentation on the presence of these scours and their potential importance for chute cutoff formation might be due to the lack of spatial and temporal resolution of morphologic datasets. Holes that occurred in chutes with natural forest cover were either stable or appeared to shrink with time, while holes that formed within farmed landscapes grew rapidly and led to chute cutoff.

Scour hole formation and growth may cause chute instability and could indicate that full cutoff is imminent. However, we documented only small amounts of erosion on the margins of the holes, likely due to detachment of the cohesive upper layer of the farmed fields the chutes are eroding through, after a year of measurements with a 5-year flood event. There was no correlation between flood peak magnitude and chute erosion over a year of UAS LiDAR scans. The presence of soil pipes draining into the large hole at Bedwell chute indicates that chute erosion is likely controlled by a combination of surface and subsurface flow events. While we could not determine the exact formative mechanism of the holes within the chute, we suggest that they are likely formed either from scour around floodplain obstacles like wood jams (Figure 15A), from collapse of soil pipes and macropores which form due to gradients in the groundwater table (Figure 15B), or a combination of the two processes.

This study indicates that scour holes will enlarge and possibly lead to chute completion if the land cover is dominated by agriculture. Scour holes in chute channels in non-agricultural settings tend to heal rather than enlarge. This mechanism for chute channel formation is distinct from upstream headcut migration, downstream embayment extension, and swale capture. Future work on river cutoffs should continue to take advantage of technological advancements in field instrumentation to produce high-resolution DEMs in numerous climatic and geologic settings. Improvements in field data can then be integrated with advanced models to improve understanding of cutoff processes.

Data Availability Statement

LiDAR data produced by the UAS has been uploaded to OpenTopography.org (https://doi.org/10.5069/G95H7DDN). Additional datasets used and/or analysed during the current study are available from the corresponding author on reasonable request.

Conflict of Interest Statement

The authors declare no conflict of interest.

References

Aberle J, Järvelä J. 2013. Flow resistance of emergent rigid and flexible floodplain vegetation. *Journal of Hydraulic Research* **51**(1): 33–45.

Abernethy B, Rutherfurd ID. 2001. The distribution and strength of riparian tree roots in relation to riverbank reinforcement. *Hydrological Processes* **15**(1): 63–79.

Allred TM, Schmidt JC. 1999. Channel narrowing by vertical accretion along the Green River near Green River, Utah. *Geological Society of America Bulletin* **111**(12): 1757–1772.

Anderson K, Gaston KJ. 2013. Lightweight unmanned aerial vehicles will revolutionize spatial ecology. *Frontiers in Ecology and the Environment* **11**(3): 138–146.

Bernatek-Jakiel A, Poesen J. 2018. Subsurface erosion by soil piping: significance and research needs. *Earth-Science Reviews* **185**: 1107–1128.

Bressan F, Papanicolaou AN, Abban B. 2014. A model for knickpoint migration in first- and second-order streams. *Geophysical Research Letters* **41**(14): 4987–4996.

Camporeale C, Perucca E, Ridolfi L. 2008. Significance of cutoff in meandering river dynamics. *Journal of Geophysical Research: Earth Surface* **113**(F1): 1-11. https://doi.org/10.1029/2006JF000694.

Carbonneau PE, Dietrich JT. 2017. Cost-effective non-metric photogrammetry from consumer-grade sUAS: implications for direct georeferencing of structure from motion photogrammetry. *Earth Surface Processes and Landforms* **42**(3): 473–486.

Charlton ME, Large AR, Fuller IC. 2003. Application of airborne LiDAR in river environments: the River Coquet, Northumberland, UK. *Earth Surface Processes and Landforms* **28**(3): 299–306.

Colomina I, Molina P. 2014. Unmanned aerial systems for photogrammetry and remote sensing: a review. *ISPRS Journal of Photogrammetry and Remote Sensing* **92**: 79–97.

Constantine JA, Dunne T. 2008. Meander cutoff and the controls on the production of oxbow lakes. *Geology* **36**(1): 23–26.

Constantine JA, McLean SR, Dunne T. 2010. A mechanism of chute cutoff along large meandering rivers with uniform floodplain topography. *Geological Society of America Bulletin* **122**(5–6): 855–869.

Czuba JA, David SR, Edmonds DA, Ward AS. 2019. Dynamics of surface-water connectivity in a low-gradient meandering river floodplain. *Water Resources Research* **55**(3): 1849–1870.

David SR, Edmonds DA, Letsinger SL. 2017. Controls on the occurrence and prevalence of floodplain channels in meandering rivers. *Earth Surface Processes and Landforms* **42**(3): 460–472.

Docker BB, Hubble TCT. 2008. Quantifying root-reinforcement of river bank soils by four Australian tree species. *Geomorphology* **100**(3–4): 401–418.

Eekhout JPC, Hoitink AJF. 2015. Chute cutoff as a morphological response to stream reconstruction: the possible role of backwater. *Water Resources Research* **51**(5): 3339–3352.

Gagliano SM, Howard PC. 1984. The neck cutoff oxbow lake cycle along the Lower Mississippi River. In *River Meandering*, Elliott CM (ed). American Society of Civil Engineers: New York; 147–158.

García-Ruiz J, Lasanta T, Alberto F. 1997. Soil erosion by piping in irrigated fields. *Geomorphology* 20(3–4): 269–278.

Gay GR, Gay HH, Gay WH, Martinson HA, Meade RH, Moody JA. 1998. Evolution of cutoffs across meander necks in Powder River, Montana, USA. *Earth Surface Processes and Landforms* 23(7): 651–662.

Han B, Endreny TA. 2014. Detailed river stage mapping and head gradient analysis during meander cutoff in a laboratory river. *Water Resources Research* 50(2): 1689–1703.

Hooke, J. M. 2004. Cutoffs galore!: occurrence and causes of multiple cutoffs on a meandering river. *Geomorphology*, 61(3-4), 225-238.

Hooke JM. 1995. River channel adjustment to meander cutoffs on the River Bollin and River Dane, northwest England. *Geomorphology* 14(3): 235–253.

Howard AD, Knutson TR. 1984. Sufficient conditions for river meandering: a simulation approach. *Water Resources Research* 20(11): 1659–1667.

Istanbulluoglu E, Bras RL, Flores-Cervantes H, Tucker GE. 2005. Implications of bank failures and fluvial erosion for gully development: field observations and modeling. *Journal of Geophysical Research: Earth Surface* 110(F1): 1-21. https://doi.org/10.1029/2004JF000145.

Jones A. 1971. Soil piping and stream channel initiation. *Water Resources Research* 7(3): 602–610.

Lawler DM. 1993. The measurement of river bank erosion and lateral channel change: a review. *Earth Surface Processes and Landforms* 18(9): 777–821.

Lejot J, Delacourt C, Piégay H, Fournier T, Trémélo ML, Allemand P. 2007. Very high spatial resolution imagery for channel bathymetry and topography from an unmanned mapping controlled platform. *Earth Surface Processes and Landforms* 32(11): 1705–1725.

Leopold LB, Langbein WB. 1966. River meanders. *Scientific American* 214(6): 60–73.

Lewis QW, Lindroth EM, Rhoads BL. 2018. Integrating unmanned aerial systems and LSPIV for rapid, cost-effective stream gauging. *Journal of Hydrology* 560: 230–246.

Lewis QW, Rhoads BL. 2018. LSPIV measurements of two-dimensional flow structure in streams using small unmanned aerial systems: 2. Hydrodynamic mapping at river confluences. *Water Resources Research* 54(10): 7981–7999.

Li Z, Wu X, Gao P. 2019. Experimental study on the process of neck cutoff and channel adjustment in a highly sinuous meander under constant discharges. *Geomorphology* 327: 215–229.

Mason J, Mohrig D. 2018. Using time-lapse lidar to quantify river bend evolution on the meandering coastal Trinity River, Texas, USA. *Journal of Geophysical Research: Earth Surface* 123(5): 1133–1144.

Micheli ER, Larsen EW. 2011. River channel cutoff dynamics, Sacramento river, California, USA. *River Research and Applications* 27(3): 328–344.

Milan DJ, Heritage GL, Hetherington D. 2007. Application of a 3D laser scanner in the assessment of erosion and deposition volumes and channel change in a proglacial river. *Earth Surface Processes and Landforms* 32(11): 1657–1674.

Moody JA, Smith JD, Ragan BW. 2005. Critical shear stress for erosion of cohesive soils subjected to temperatures typical of wildfires. *Journal of Geophysical Research: Earth Surface* 110(F1): 1-13. https://doi.org/10.1029/2004JF000141.

Moore WL, Masch FD, Jr. 1962. Experiments on the scour resistance of cohesive sediments. *Journal of Geophysical Research* 67(4): 1437–1446.

Opperman JJ, Luster R, McKenney BA, Roberts M, Meadows AW. 2010. Ecologically functional floodplains: connectivity, flow regime, and scale. *Journal of the American Water Resources Association* 46(2): 211–226.

Orr CH, Stanley EH, Wilson KA, Finlay JC. 2007. Effects of restoration and reflooding on soil denitrification in a leveed Midwestern floodplain. *Ecological Applications* 17(8): 2365–2376.

Parsons, D. R., Jackson, P. R., Czuba, J. A., Engel, F. L., Rhoads, B. L., Oberg, K. A., ... Riley, J. D. 2013. Velocity Mapping Toolbox (VMT): a processing and visualization suite for moving-vessel ADCP measurements. *Earth Surface Processes and Landforms*, 38(11), 1244-1260.

Richards, D., & Konsoer, K. 2019. Morphologic adjustments of actively evolving highly curved neck cutoffs. *Earth Surface Processes and Landforms*.

Schumm SA. 1963. Sinuosity of alluvial rivers on the Great Plains. *Geological Society of America Bulletin* 74(9): 1089–1100.

Schwenk J, Foufoula-Georgiou E. 2016. Meander cutoffs nonlocally accelerate upstream and downstream migration and channel widening. *Geophysical Research Letters* 43(24): 12 437–12 445.

Stølum HH. 1996. River meandering as a self-organization process. *Science* 271(5256): 1710–1713.

Tarolli P. 2014. High-resolution topography for understanding Earth surface processes: opportunities and challenges. *Geomorphology* 216: 295–312.

Thielicke W, Stamhuis E. 2014. PIVlab – towards user-friendly, affordable and accurate digital particle image velocimetry in MATLAB. *Journal of Open Research Software* 2(1): 1-10. https://doi.org/10.5334/jors.bl.

Van Dijk WM, Schuurman F, van de Lageweg WI, Kleinhans MG. 2014. Bifurcation instability and chute cutoff development in meandering gravel-bed rivers. *Geomorphology* 213: 277–291.

Viero DP, Dubon SL, Lanzoni S. 2018. Chute cutoffs in meandering rivers: formative mechanisms and hydrodynamic forcing. In *Fluvial Meanders and Their Sedimentary Products in the Rock Record*, Ghinassi M, Colombera L, Mountney NP, Reesink AJH, Bateman M (eds). Wiley: New York; 201–229.

Wiberg PL, Smith JD. 1987. Calculations of the critical shear stress for motion of uniform and heterogeneous sediments. *Water Resources Research* 23(8): 1471–1480.

Woodget AS, Austrums R, Maddock IP, Habit E. 2017. Drones and digital photogrammetry: from classifications to continuums for monitoring river habitat and hydromorphology. *Wiley Interdisciplinary Reviews: Water* 4(4): 1-20, e1222.

Zinger JA, Rhoads BL, Best JL. 2011. Extreme sediment pulses generated by bend cutoffs along a large meandering river. *Nature Geoscience* 4(10): 675-678.